iScience

CellPress
OPEN ACCESS

Article

Flux upcycling of spent NMC 111 to nickel-rich NMC cathodes in reciprocal ternary molten salts

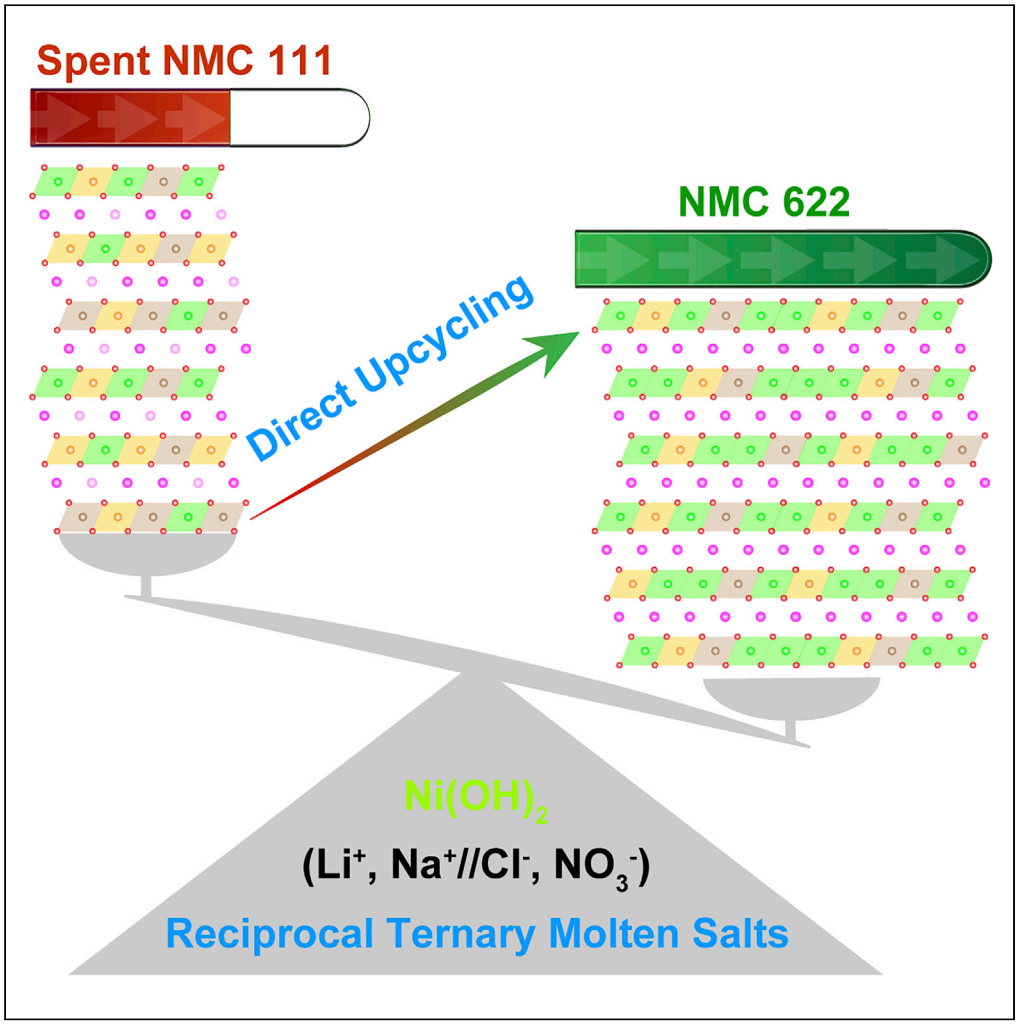

Tao Wang, Huimin Luo, Juntian Fan, Bishnu P. Thapaliya, Yaocai Bai, Ilias Belharouak, Sheng Dai

dais@ornl.gov

Highlights

A "reciprocal ternary molten salts" (RTMS) system is developed for upcycling

Directly upcycling of spent NMC 111 to Ni-rich NMC (NMC 622) is realized in air

RTMS provides the Li source and a flux oxygen-rich environment for upcycling

Wang et al., iScience 25, 103801
February 18, 2022
https://doi.org/10.1016/j.isci.2022.103801

iScience

CellPress
OPEN ACCESS

Article

Flux upcycling of spent NMC 111 to nickel-rich NMC cathodes in reciprocal ternary molten salts

Tao Wang,[1,2] Huimin Luo,[3] Juntian Fan,[2] Bishnu P. Thapaliya,[1] Yaocai Bai,[4] Ilias Belharouak,[4] and Sheng Dai[1,2,5,*]

SUMMARY

The proper handling of end-of-life (EOL) lithium-ion batteries (LIBs) has become an urgent and challenging issue with the surging use of LIBs, in which recovering high-value cathodes not only relieves the pressure on the raw material supply chain but also minimizes environmental pollution. Beyond direct recycling of spent cathodes to their pristine states, the direct upcycling of spent cathodes to the next-generation cathodes is of great significance to maximize the value of spent materials and to sustain the fast development of LIBs. Herein, a "reciprocal ternary molten salts" (RTMS) system was developed to directly upcycle spent NMC 111 to Ni-rich NMCs by simultaneously realizing the addition of Ni and the relithiation of Li in spent NMC 111. After RTMS flux upcycling, the obtained Ni-rich NMCs exhibited an α-$NaFeO_2$-type layered structure, restored Li content, and excellent performance, which is very similar to that of the pristine NMC 622.

INTRODUCTION

Lithium-ion batteries (LIBs) are widely used in portable devices and electrical vehicles because of their high energy density, which has changed people's lifestyle in last decades (Manthiram, 2017, 2020; Yoshino, 2012). The cumulative lithium-ion battery demand has soared from 0.5 GW-hours (GWh) in 2010 to 526 GWh in 2020, and been predicted to 9300 GWh in 2030 (Statista, 2020). To meet this high demand, minerals containing lithium, cobalt, manganese, and nickel are massively needed and becoming a bottle neck in scale-up production of commercial lithium nickel manganese cobalt oxide ($LiNi_xMn_yCo_zO_2$, $x + y + z = 1$) cathodes, resulting in constantly increasing costs from raw materials (Robinson, 2020; Olivetti et al., 2017). Along with the scaled production of LIBs, end-of-life (EOL) LIBs are causing serious environmental contaminations due to their hazardous components, such as toxic lithium compounds, heavy metals, and electrolytes (Wang et al., 2020; Duarte Castro et al., 2021; Bai et al., 2020). Recovering materials especially high-value cathodes from EOL LIBs not only relieves the pressure on the raw material supply chain but also minimizes environmental pollution of EOL LIBs (Mossali et al., 2020; Chen et al., 2019; Du et al., 2021). Most of current facilities and processes to recover EOL LIBs are to recover valuable metals, especially cobalt by pyrometallurgical and hydrometallurgical recycling methods (Ciez and Whitacre, 2019; Mansur et al., 2021; Atia et al., 2019; Velázquez-Martínez et al., 2019). Though the recovered metals can serve as raw materials in supply chains, the destruction of cathode materials consumes significant energy and results in the loss of compound structure added value (Zhang et al., 2018a; Li et al., 2018a; Gao et al., 2017). Moreover, the resynthesis of cathode compounds from metals requires energy-intensive processes, which incur extra costs and greenhouse gas emissions (Ciez and Whitacre, 2019). To overcome the drawbacks of pyrometallurgical and hydrometallurgical recycling process, direct recycling stands out as an emerging technology to retrain the added value of compound structure by healing the compositional and structural defects in spent cathode materials, or using the spent graphite anodes for other energy storage devices, such as Na/K-ion batteries (Yang et al., 2020; Xu et al., 2020; Li et al., 2020; Larouche et al., 2020; Sloop et al., 2018; Fan et al., 2021; Liang et al., 2019; Divya et al., 2020; Meng et al., 2022). As the main force of cathode materials, NMC cathodes keep changing their chemical compositions to pursue lower cost, higher capacity, and cycling stability (Manthiram, 2020; 2018b). For example, $LiCoO_2$, proposed as the cathode materials by Prof. John B. Goodenough in 1980s, was widely used in portable devices (Mizushima et al., 1980; Lyu et al., 2021). Nowadays, $LiNi_{1/3}Mn_{1/3}Co_{1/3}O_2$ (NMC 111) with a lower content of Co takes the baton from $LiCoO_2$ to achieve balanced cost, capacity, and stability for commercial automotive LIBs (Ding et al., 2019). The next-generation cathodes of automotive LIBs were predicted as Ni-rich and Co-lean cathodes (e.g. NMC 622, NMC 811) for replacing present NMC 111 in the near future (Noh et al.,

[1]Chemical Sciences Division, Oak Ridge National Laboratory, Oak Ridge, TN 37831, USA

[2]Department of Chemistry, The University of Tennessee, Knoxville, TN 37916, USA

[3]Manufacturing Science Division, Oak Ridge National Laboratory, Oak Ridge, TN 37831, USA

[4]Electrification and Energy Infrastructures Division, Oak Ridge National Laboratory, Oak Ridge, TN 37831, USA

[5]Lead contact

*Correspondence: dais@ornl.gov

https://doi.org/10.1016/j.isci.2022.103801

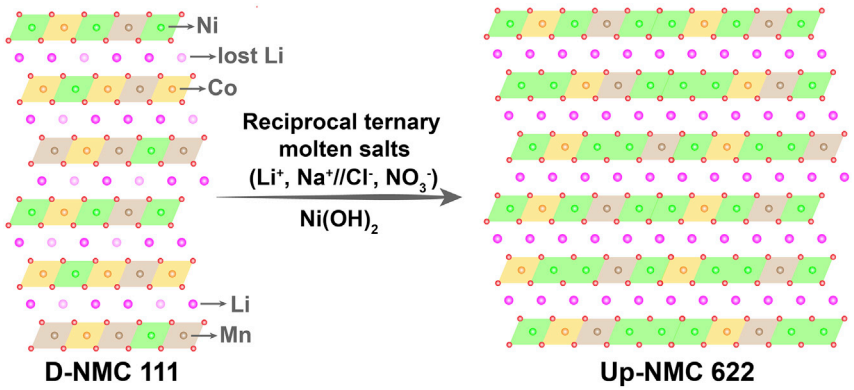

Scheme 1. Illustration of the upcycling of D-NMC 111 to Up-NMC 622 in RTMS

2013; Yoon et al., 2015; Kim et al., 2020). The direct recycling of spent cathodes to their pristine states easily falls behind the fast development of cathode materials, because recycling of EOL LIBs generally happens years later after production (Beaudet et al., 2020; 2018b). Thus, beyond direct recycling, direct upcycling of spent cathodes to the next-generation cathodes is critical to maximize the value of spent materials.

Here, targeting the direct upcycling of spent NMC 111 to Ni-rich NMC cathodes, we developed a "reciprocal ternary molten salts" (RTMS) system to simultaneously realize the addition of Ni and relithiation in spent NMC 111, where RTMS are those molten salts containing two cation species and two anion species. Because the irreversible structure change in spent NMC is mainly caused by irreversible Li loss, the relithiation process is critical and has been achieved in some direct recycling works by flux methods (Wang et al., 2020; Shi et al., 2019). Li containing flux media (eutectic molten salts or ionic liquids) can serve as both Li sources and solvents to restore Li in spent NMC under relatively low temperatures (below 300°C), because the highly charged flux media favor for transporting ionic reactants (Li et al., 2016; Yuan et al., 2018; Parnham and Morris, 2007). However, the upcycling of spent NCM 111 to Ni-rich NMC is still challenging by those reported flux methods. Unlike the slight weight change during the direct relithiation process, a significant weight change of NMC will happen during the upcycling process. For example, the upcycling of NMC 111 to NMC 622 will almost double the weight of NMC 111 from the insertion of Li, Ni, and O, which requires a high temperature above 600°C to construct the α-$NaFeO_2$-type layered structure. Besides, an oxygen-rich environment is essential to the sufficient oxidation of inserted Ni^{2+} to Ni^{3+}, to minimize lattice oxygen vacancies and Li/Ni antisite defects in Ni-rich NMC (Mesnier and Manthiram, 2020). The reversible reaction: $NaNO_3 + LiCl \rightleftharpoons LiNO3 + NaCl$ in the Li^+, $Na^+||Cl^-$, NO_3^- RTMS system enables a low eutectic melting point for the effective flux process under 300°C. Though nitrates will decompose above 600°C, the residual LiCl/NaCl can still provide a flux media for the formation of layered NMC structure under even higher temperature. Thus, a Li^+, $Na^+||Cl^-$, NO_3^- RTMS system that can work in a wide temperature range and provide an oxygen-rich environment was developed here for the upcycling of spent NMC 111 to Ni-rich NMC (Scheme 1). In this upcycling strategy, cost-effective lithium chloride and nickel nitrate were chosen as Li and Ni sources, respectively. Sodium hydroxide was used to react with nickel nitrate to obtain nickel hydroxide precursor and sodium nitrate for RTMS. After flux upcycling, the obtained Ni-rich NMC products (named as Up-NMC 622 based on its chemical composition) exhibited pure α-$NaFeO_2$-type layered structure, restored Li content, and excellent electrochemical performance, which is very similar to that of the pristine NMC 622. The successful upcycling of spent NMC 111 provides a novel flux method to achieve the direct upcycling of spent LIB cathodes to the next-generation cathodes.

RESULTS

The upcycling of spent NMC 111 to Ni-rich NMCs requires not only the addition of Li, Ni, and O but also the formation of the α-$NaFeO_2$-type layered structure. Compared to the direct relithiation, the addition of Ni in NMCs is more challenging, because the general $Ni(OH)_2$ precursor is insoluble in common solvents and the Ni^{2+} in Ni source needs to be oxidized to Ni^{3+} to form a Ni-rich layered structure. The Li^+, $Na^+||Cl^-$, NO_3^- RTMS system can provide Li source for relithiation and an oxygen-rich environment for the oxidation of Ni^{2+} to Ni^{3+}, which is critical for the realization of upcycling. To obtain a uniform dispersion of $Ni(OH)_2$ in RTMS system, $Ni(OH)_2$ precursor and $NaNO_3$ in RTMS are *in situ* synthesized by the reaction of $Ni(NO_3)_2 \cdot 6H_2O$

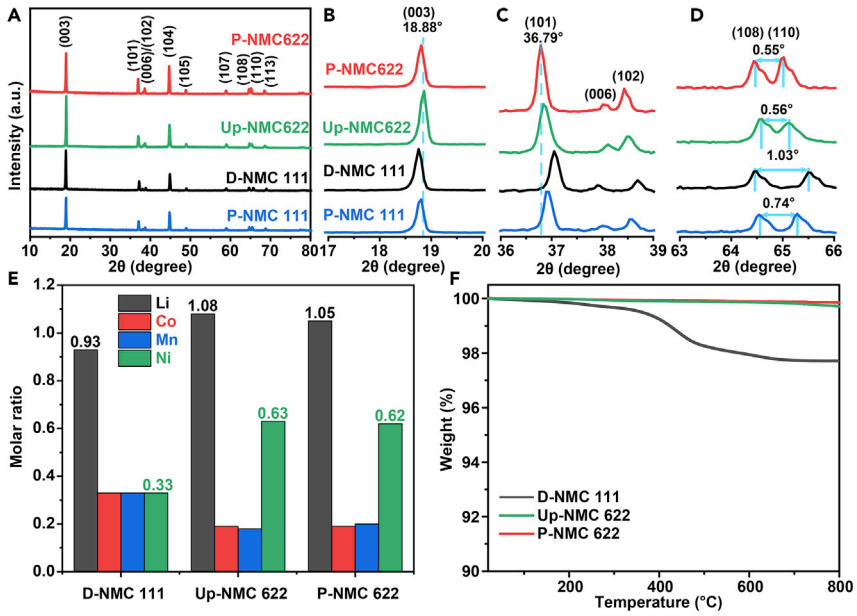

Figure 1. Structures and chemical compositions of NMCs

(A–D) XRD patterns showing survey spectrum (A) and zoom-in peaks (B-D) of D-NMC 111, P-NMC 111, P-NMC 622, and Up-NMC 622.

(E) Metal molar ratios of D-NMC 111, P-NMC 622, and Up-NMC 622 based on ICP results.

(F) TGA curves of D-NMC 111, P-NMC 622, and Up-NMC 622

with NaOH. A chemical delithiated NMC 111 (named as D-NMC 111) instead of the spent materials from EOL LIBs is used as the model materials for the optimization of upcycling conditions, where some other factors such as cathode electrolyte interaction are eliminated. For the upcycling of D-NMC 111 to NMC 622, a slurry is formed when milling D-NMC 111:$Ni(NO_3)_2{\cdot}6H_2O$:LiCl:NaOH under a mass ratio of 1:2.4:0.86:1.2. The slurry was dried under 110°C in a vacuum oven, and heated to 300°C for 5 h, then to 800°C for 5 h in a muffle furnace. Then, the obtained NMC-RTMS was washed with water to remove RTMS and reheated to 600°C for 2 h in air to yield the final product (named as Up-NMC 622). The pristine commercial NMC 111 and NMC 622 were used as references, and named as P-NMC 111 and P-NMC 622, respectively. As we reported previously (Wang et al., 2020), D-NMC 111 had a chemical composition of $Li_{0.93}Ni_{0.33}Co_{0.33}Mn_{0.33}O_2$ calculated from inductively coupled-plasma optical emission spectroscopy (ICP-OES) results. After upcycling, the chemical composition of Up-NMC 622 is $Li_{1.08}Ni_{0.63}Co_{0.19}Mn_{0.18}O_2$ (Figure 1E), almost coincides with that of P-NMC 622 ($Li_{1.05}Ni_{0.62}Co_{0.19}Mn_{0.20}O_2$), suggesting the successful upcycling in chemical composition. The crystal structure and thermal stability of NMCs can be investigated by X-ray diffraction (XRD) and thermogravimetric analysis (TGA), respectively. Both pristine NMC 111 and NMC 622 have the O3-type structure similar to the layered structure of α-$NaFeO_2$. Their XRD peaks are indexed according to α-$NaFeO_2$ (Figure 1A). Though D-NMC 111 maintains the similar O3-type structure to pristine NMC 111 (P-NMC 111), peak shifts can be identified in their XRD patterns. The (108) and (110) diffraction peaks of D-NMC 111 shift away from each other (Figure 1D), and the (003) peak slightly shifts to lower angles compared to those of P-NMC 111 (Figure 1B), because the positively charged MO_6 slabs in D-NMC 111 lead to the expansion of the *c* parameter. Compared to D-NMC 111 and P-NMC 111, P-NMC 622 has a narrower peak splitting between (108) and (110) of 0.45°due to its higher Ni content (Figure 1D). The XRD patterns of Up-NMC 622 and P-NMC 622 reveal same features that their (003) peaks slightly shift to higher angles compared to D-NMC 111 (Figure 1B), and (104) peak to lower angles (Figure 1C). The split between (108) and (110) in XRD pattern of Up-NMC 622 is similar to that of P-NMC 622 (0.56° vs 0.55°), suggesting its well layered structure. Those XRD results validate the structure upcycling of D-NMC 111 to Up-NMC 622. Besides, D-NMC 111 exhibits a weight loss of 2.3% at 800°C in TGA curve (Figure 1F), mainly from the oxygen evolution during surface reconstruction. The TGA curves of Up-NMC 622 and P-NCM 622 are almost identical, indicating their similar thermal stability. The changes in morphology and elemental distribution of NMCs during the upcycling process were characterized by a scanning electron microscope (SEM) with energy-dispersive spectroscopy (EDS). As shown in Figures 2A, 2C, and S1, Up-NMC 622 reveals

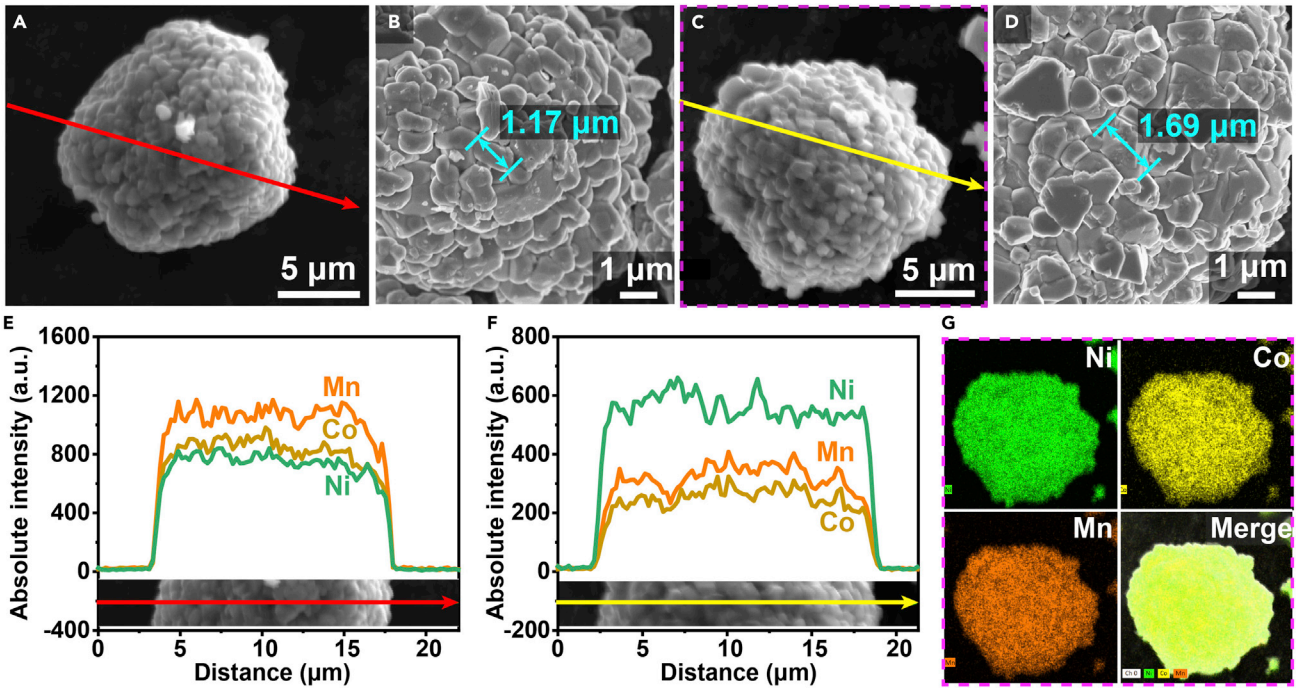

Figure 2. Morphologies and element distributions of D-NMC 111 and Up-NMC 622

(A–D) SEM images of D-NMC 111 (A and B) and Up-NMC 622 (C and D).

(E–F) SEM-EDS line scans of D-NMC 111 (E) and Up-NMC 622 (F).

(G) SEM-EDS elemental mappings of Up-NMC 622

similar secondary particles to D-NMC 111, which are aggregations of primary microparticles with random sizes and grain orientations. In zoom-in SEM images (Figures 2B, 2D, and S2), the primary particles of Up-NMC 622 becomes larger than those of D-NMC 111, suggesting a growth of primary particles during the upcycling process. SEM-EDS line scan was performed to investigate the element distribution across the secondary particles (Figures 2E and 2F). In D-NMC 111, Mn has slightly stronger signal intensity than Ni and Co. While in Up-NMC 622, Ni reveals much stronger signal intensity than Mn and Co through the whole particle, indicating the insertion of Ni in particles during the upcycling process. Moreover, the distribution of Ni is uniform with the same shape as those of Co and Mn in SEM-EDS mapping (Figure 2G). Based on the ICP, XRD, TGA, and SEM results, the upcycling of D-NMC 111 to Up-NMC 622 is successful in both chemical composition and crystal structure.

To evaluate the electrochemical performance of NMCs, they were used as active materials in cathodes, and paired with Li foil or graphite anodes for half-cell or full-cell tests, respectively. The half-cells were tested at the same current density of 20 mA/g in a voltage range of 3–4.3 V. As shown in Figure 3A and Table S1, the first charge capacity of D-NMC 111 is only 140.5 mAh/g, much lower than that of P-NMC 111 (161.9 mAh/g), due to the delithiated nature of D-NMC 111. The recovered discharge capacity of D-NMC 111 reveals the electrochemical relithiation from the excessive lithium in Li foil (Figures 3A and 3B), which always happens in a half-cell test (Ganter et al., 2014). That is why the first charge capacity rather than the discharge capacity is used as a critical parameter in half-cell tests to investigate the amount of active Li species in cathodes. After upcycling, the first charge capacity of Up-NMC 622 is close to that of commercial P-NMC 622 (195.4 vs 197.3 mAh/g). In general, the successful direct relithiation of D-NMC 111 can achieve a comparable charge capacity to P-NMC 111 (Wang et al., 2020). Here, beyond the direct relithiation, Up-NMC 622 exhibits a much higher first charge capacity than P-NMC 111 (195.4 vs 161.9 mAh/g), indicating an upcycling in electrochemical performance. In addition, the charge-discharge capacities of Up-NMC 622 are close to those of P-NMC 622 (Figure 3C), and much larger than those of P-NMC 111 and D-NMC 111 during 100 cycles, validate the sustainable superior performance of Up-NMC 622 in half-cell tests. To eliminate the interference of electrochemical relithiation on discharge capacities, commercial graphite was employed as anodes for full-cell tests, because graphite will not supply extra Li during the discharge processes. A high loading of

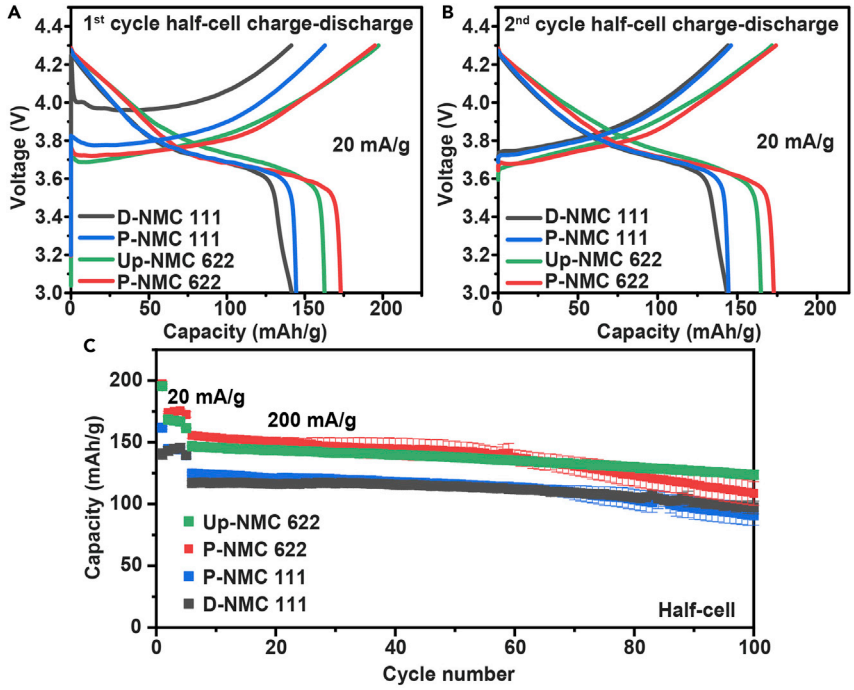

Figure 3. Half-cell performance of NMCs

(A) The first cycle charge/discharge curves of NMCs for half-cell tests.

(B) The second cycle charge/discharge curves of NMCs for half-cell tests.

(C) Cycle performance of NMCs for half-cell tests (Error bars are standard deviations).

the cathode active material about 7 mg/cm^2 was used to simulate the situation as practical as possible. The full cells were activated at 20 mA/g for four cycles before cycling at 200 mA/g in a voltage range of 3–4.2 V. The initial open-circuit voltage of full-cell is around 0 V, thus the first charge process was from 0 to 4.2 V. As shown in Figure 4A and Table S2, D-NMC 111 does not exhibit the electrochemical relithiation during the first discharge process, whose first discharge capacity is only 119.5 mAh/g, much lower than that of P-NMC 111 (139.5 mAh/g), while the first charge/discharge capacities of Up-NMC 622 are larger than those of P-NMC 111 (charge capacity: 188.6 vs 170.1 mAh/g; discharge capacity: 153.6 vs 139.5 mAh/g at 20 mA/g). Moreover, Up-NMC 622 exhibited higher capacities than P-NMC 111 and D-NMC 111 over 100 cycles at a higher specific current of 200 mA/g (Figure 4C). Thus, Up-NMC 622 upcycled from D-NMC 111 has a better electrochemical performance as a LIB cathode than P-NCM 111; therefore, the RTMS flux method is effective for the upcycling of D-NMC 111 to NMC 622.

The upcycling of D-NMC 111 to NMC 811 was also tried by RTMS flux method using D-NMC 111:Ni(NO_3)$_2$·6H_2O:LiCl:NaOH under a mass ratio of 1:6.4:2.12:1.8. After upcycling, the chemical composition of Up-NMC 811 is $Li_{1.08}Ni_{0.79}Co_{0.11}Mn_{0.10}O_2$ (Figure S5E), almost coincides with that of P-NMC 811 ($Li_{1.07}Ni_{0.76}Co_{0.12}Mn_{0.12}O_2$), suggesting the successful upcycling of chemical composition. According to XRD patterns (Figure S5A), both pristine NMC 811 and Up-NMC 811 have the O3-type structure similar to the layered structure of α-$NaFeO_2$. P-NMC 811 has a narrow peak splitting between (108) and (110) of 0.45°due to its high Ni content. The XRD patterns of Up-NMC 811 and P-NMC 811 reveal same features that their (003) peaks slightly shift to higher angles compared to D-NMC 111, and (104) peak to lower angles. The split between (108) and (110) in XRD pattern of Up-NMC 811 is 0.42° similar to that of P-NMC 811, suggesting its well layered structure. The TGA curves of Up-NMC 811 and P-NCM 811 almost coincide (Figure S5F), indicating their similar thermal stability. The electrochemical performance of Up-NMC 811 was investigated by half-cell tests, using a specific current density of 20 mA/g in a voltage range of 3–4.3 V. As shown in Figure S6 and Table S1, the first charge capacity of Up-NMC 811 is almost the same as that of P-NMC 811 (215.2 vs 216.2 mAh/g). However, the coulombic efficiency of Up-NMC 811 is lower than that of P-NMC 811, resulting in a low discharge capacity (153.7 mAh/g). Though Up-NMC 811 is not as good as P-NMC 811 in battery performance, Up-NMC 811 still has upgraded charge-discharge capacities

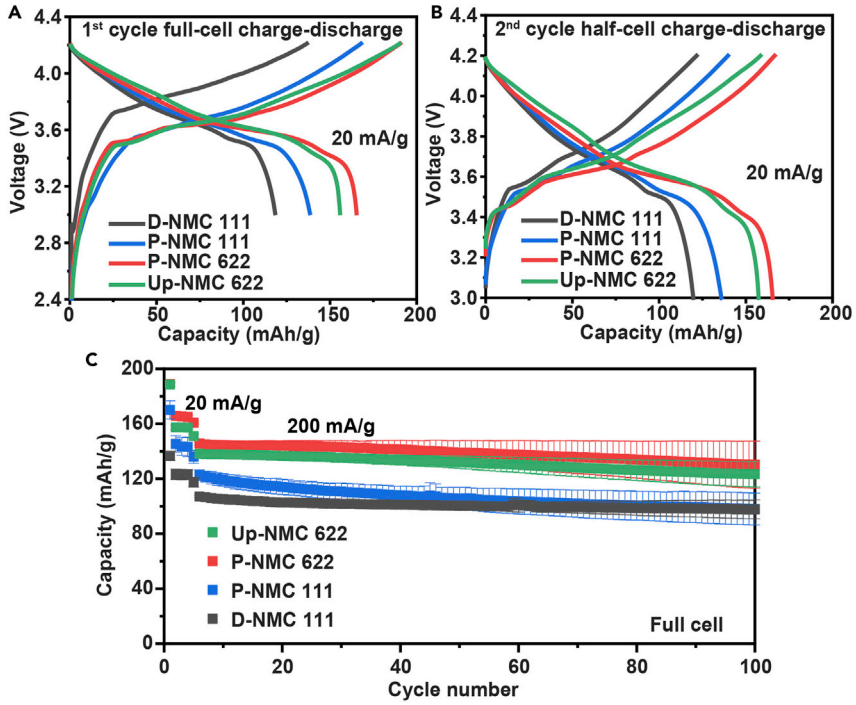

Figure 4. Full-cell performance of NMCs

(A) The first cycle charge/discharge curves of NMCs for full-cell tests.

(B) The second cycle charge/discharge curves of NMCs for full-cell tests.

(C) Cycle performance of NMCs for full-cell tests (Error bars are standard deviations).

compared to P-NMC 111 and D-NMC 111. The low coulombic efficiency of Up-NMC 811 may be due to its large grain size (Figures S7D–S7F). Up-NMC 811 does not reveal the typical secondary particles like P-NMC 811 in SEM images (Figure S7), suggesting the dissolution of D-NMC 111 in RTMS during the upcycling process. The SEM-EDS line scan (Figure S7H) and element mapping (Figure S7G) validate the uniform distribution of Ni, Co, and Mn in Up-NMC 811. Based on the above results, the upcycling of D-NMC 111 to Up-NMC 811 are also successful in both chemical composition and crystal structure.

To shed light on the upcycling process, TGA and DTA curves of the upcycling mixture for Up-NMC 622 were collected after vacuum dry process. As shown in Figure 5, TGA curves of the upcycling mixture and $NaNO_3$/LiCl salts both have a major weight loss above 520°C, corresponding to the decomposition of nitrates. Besides, the upcycling mixture exhibited a weight loss of 2.5% in TGA curve and an endothermic peak in DTA curve at around 166°C, corresponding to the decomposition of $Ni(OH)_2$. The other endothermic peak in DTA curve of the upcycling mixture locates at around 264°C, where no weight loss is observed in TGA curve, corresponding to the melting point of RTMS. The low melting point of RTMS enables an effective flux process when heating the upcycling mixture to 300°C. Though nitrates decompose at around 520°C, the residual binary molten salts NaCl/LiCl can still work as a flux media at 800°C. That is why the upcycling mixture is heated to 300°C and then to 800°C to achieve a successful upcycling. To highlight the importance of RTMS, we designed control experiments using $NaNO_3$/$LiNO_3$, NaCl/LiCl, or LiCl/$LiNO_3$ binary molten salts. As shown in Figure 6B, the product using NaCl/LiCl exhibited mixed phases in XRD pattern, where the impurity was assigned to $Li_2Ni_8O_{10}$. The formation of $Li_2Ni_8O_{10}$ with a low oxidation state of Ni is due to the absence of oxygen-rich environment from nitrate salts. The use of LiCl/$LiNO_3$ molten salts resulted in the impurity of $LiNiO_2$ in product (Figure 6B), suggesting the separate nucleation and growth of $LiNiO_2$ particles. The product obtained in $LiNO_3$/$NaNO_3$ binary molten salts exhibited a pure α-$NaFeO_2$-type layered structure in XRD pattern (Figure 6A), but the two pair of fused (006)/(102) and (008)/(110) peaks indicated a defective layered structure (Figures 6B and 6C). Because $LiNO_3$ and $NaNO_3$ will completely decompose above 600°C, $LiNO_3$/$NaNO_3$ binary molten salts cannot provide effective flux process under high temperature. The Li molar ratios of products synthesized in LiCl/NaCl, LiCl/$LiNO_3$, $LiNO_3$/$NaNO_3$, and RTMS are calculated as 0.63, 0.88, 1.04, and 1.09, respectively, according to their ICP results (Figure 4D and Table S3). In another control experiment, $Ni(OH)_2$ was directly mixed with $Na(NO_3)_2$ and LiCl, and grinded

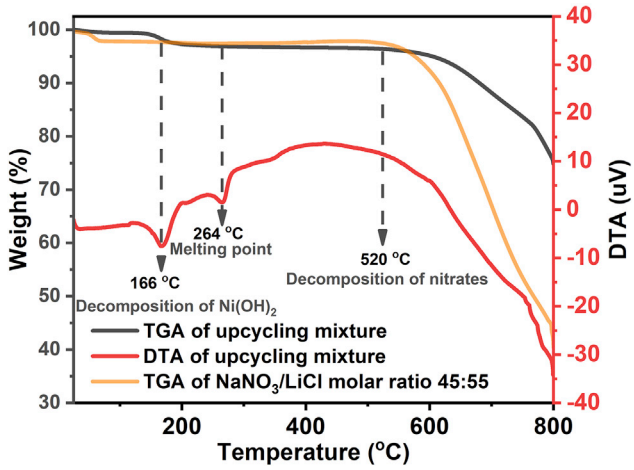

Figure 5. TGA and DTA curves of upcycling mixture

to form a uniform mixture. The corresponding product was denoted as Up-NMC 622-$Ni(OH)_2$. As shown in Figure S4, Up-NMC 622-$Ni(OH)_2$ exhibited the α-$NaFeO_2$-type layered structure, similar to Up-NMC 622. However, the split between (108) and (110) in XRD pattern of Up-NMC 622-$Ni(OH)_2$ is 0.79°, much larger than those of Up-NMC 622 (0.56°) and P-NMC 622 (0.55°), indicating a lower Ni content in lattice. The SEM images (Figure S3) of Up-NMC 622-$Ni(OH)_2$ reveal some attached nanoparticles on primary particles, which is not found in Up-NMC 622. Those nanoparticles may from the individually nucleation of Ni-related species. Moreover, in half-cell tests, the first charge capacity of Up-NMC 622-$Ni(OH)_2$ is smaller than that of Up-NMC 622 (183.3 vs 195.4 mAh/g, Table S1), indicating that the *in situ* synthesis of $Ni(OH)_2$ during the upcycling process is conducive to the diffusion of Ni in NMC lattice to form a uniform product with a better battery performance. Based on the above results, nitrate salts are critical to achieve full lithiation during flux process by oxidizing Ni^{2+} to Ni^{3+}. Chloride salts can provide a flux media under high temperature to promote the diffusion of Ni into NMC structure, because molten chlorides have a good capacity to solubilize metallic cations of oxides (Onofre, 2019). In addition, the use of mixed alkaline metal cations Li^+ and Na^+ is conducive to achieve a lower melting point and an effective flux process. The use of RTMS is critical for the successful upcycling of D-NMC 111 to NMC 622 and NMC811 in both structure and chemical composition.

DISCUSSION

In conclusion, the successful upcycling of D-NMC 111 to Ni-rich NMC cathodes was achieved under ambient pressure and air atmosphere via an RTMS flux upcycling strategy. The Li^+, $Na^+||Cl^-$, NO_3^- RTMS featuring a low melting point can simultaneously provide the Li source, an oxygen-rich environment for the oxidation of Ni^{2+} to Ni^{3+}, and effective flux media under high temperature, which are essential for the successful upcycling. Up-NMC 622 has nearly identical chemical composition and structure to P-NMC 622, whose electrochemical performance as a LIB cathode is better than those of D-NMC 111 and P-NMC 111. The RTMS upcycling strategy is promising for the upcycling of spent NMC cathodes to the next-generation Ni-rich NMC cathodes.

LIMITATION OF THE STUDY

In this work, we provided an RTMS flux upcycling strategy to realize the successful upcycling of D-NMC 111 to NMC 622 in air. However, the upcycling of D-NMC 111 to NMC 811 is still challenging. Though the RTMS flux upcycling strategy is good enough to achieve Up-NMC 811 with the very similar chemical composition and crystal structure to P-NMC 811, the initial coulombic efficiency of Up-NMC 811 is not as high as that of P-NMC 811 in half-cell tests. The low coulombic efficiency of Up-NMC 811 is mainly due to its large grain size with the significant increase in mass during upcycling processes. Thus, the morphology control is also important for a successful upcycling. Besides, instead of the actual waste materials from EOL LIBs, chemically delithiated NMC 111 (D-NMC 111) materials were used as the model materials for the optimization of upcycling conditions, where some other factors such as cathode electrolyte interaction are eliminated, because the spent materials from EOL LIBs vary in structure and chemical composition degradations, which can hardly keep consistent for control experiments. As loss in lithium inventory is a major mechanism in

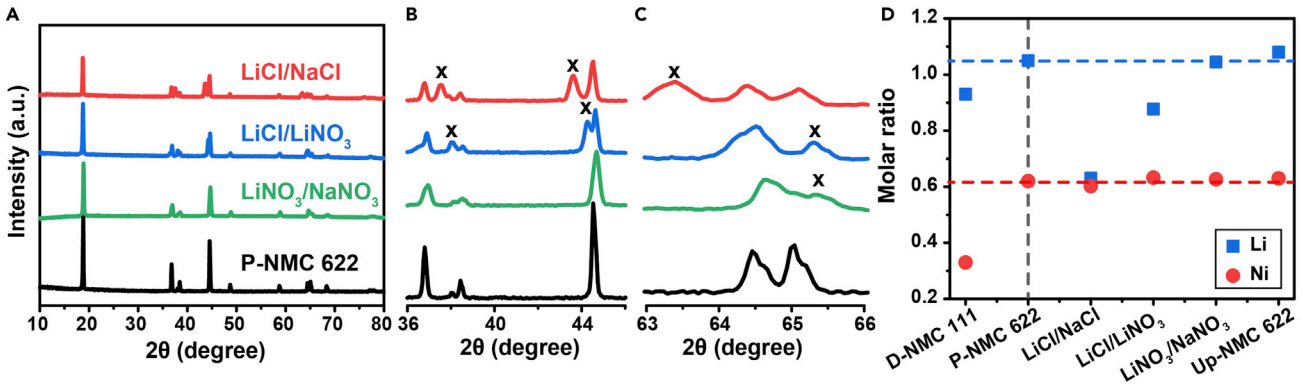

Figure 6. Comparison of binary molten salts for upcycling

(A–C) XRD patterns showing survey spectrum (A) and zoom-in peaks (B–D) of P-NMC 111 and products obtained from different binary molten salts. The peaks from impurities are marked as "X" in (B) and (C).

(D) Metal molar ratios of D-NMC 111 and P-NMC 622 products obtained from different binary molten salts, and Up-NMC 622 based on ICP results

capacity fade, the principle of upcycling the delithiated NMC should be similar. In addition, this work is a part of Re-Cell projects (https://recellcenter.org/), a $15 million center launched by DOE in 2019. For the comparison purpose, all projects within the center use the same chemically delithiated materials. As it is challenging to generate large quantity and consistent actual waste materials, Re-Cell chose to create the delithiated material via chemical delithiation method, which is much faster, easier to scale up and to have each group use the same control samples so that different upcycling protocols can be compared scientifically in the current stage. After the optimization of all the upcycling conditions, the actual waste materials will be used in the next stage.

STAR★METHODS

Detailed methods are provided in the online version of this paper and include the following:

- KEY RESOURCES TABLE
- RESOURCE AVAILABILITY
  - Lead contact
  - Materials availability
  - Data and code availability
- METHOD DETAILS
  - Upcycling procedures
  - Electrochemical measurements
  - Characterizations
- QUANTIFICATION AND STATISTICAL ANALYSIS

SUPPLEMENTAL INFORMATION

Supplemental information can be found online at https://doi.org/10.1016/j.isci.2022.103801.

ACKNOWLEDGMENTS

This research was performed through the Re-Cell Center, which gratefully acknowledges support from the U. S. Department of Energy (DOE), Office of Energy Efficiency and Renewable Energy, and the Vehicle Technologies Office. The authors thank Dr. Kris Pupek, Dr. Erik Dahl, and Dr. Bryant Polzin from Argonne National Laboratory for providing pristine and delithiated NMC 111. This manuscript was authored by UT-Battelle, LLC under Contract No. DEAC05-00OR22725 with the U.S. Department of Energy. This article has been contributed to by US Government employees and their work is in the public domain in the USA. The Department of Energy will provide public access to these results of federally sponsored research by the DOE Public Access Plan.

AUTHOR CONTRIBUTIONS

Conceptualization, SD; Methodology, T.W.; Investigation, T.W.; Writing – Original Draft, T.W.; Writing – Review & Editing, T.W., H. L., and SD; Funding Acquisition, H.L. and SD; Resources, B.P.T., Y.B., J.F., I. B., and H.L.; Supervision, SD

DECLARATION OF INTERESTS

The authors declare no competing interests.

Received: October 19, 2021
Revised: December 21, 2021
Accepted: January 19, 2022
Published: February 18, 2022

REFERENCES

Manthiram, A. (2017). An outlook on lithium ion battery technology. ACS Cent. Sci. *3*, 1063–1069. https://doi.org/10.1021/acscentsci.7b00288.

Yoshino, A. (2012). The birth of the lithium-ion battery. Angew. Chem. Int. Ed. *51*, 5798–5800. https://doi.org/10.1002/anie.201105006.

Manthiram, A. (2020). A reflection on lithium-ion battery cathode chemistry. Nat. Commun. *11*, 1550. https://doi.org/10.1038/s41467-020-15355-0.

Statista (2020). Statista High Demand for Lithium-Ion Batteries (Statista Inc.). https://www.statista.com/chart/23808/lithium-ion-battery-demand.

Robinson, D. (2020). Supply Chain Bottleneck Strangling Scale-Up of Lithium-Ion Battery Production for EVs (NS ENERGY). https://www.nsenergybusiness.com/features/lithium-ion-batteries-electric-vehicles/.

Olivetti, E.A., Ceder, G., Gaustad, G.G., and Fu, X. (2017). Lithium-ion battery supply chain considerations: analysis of potential bottlenecks in critical metals. Joule *1*, 229–243. https://doi.org/10.1016/j.joule.2017.08.019.

Wang, T., Luo, H., Bai, Y., Li, J., Belharouak, I., and Dai, S. (2020). Direct recycling of spent NCM cathodes through ionothermal lithiation. Adv. Energy Mater. *10*, 2001204. https://doi.org/10.1002/aenm.202001204.

Duarte Castro, F., Vaccari, M., and Cutaia, L. (2021). Valorization of resources from end-of-life lithium-ion batteries: a review. Crit. Rev. Environ. Sci. Technol. 1–44. https://doi.org/10.1080/10643389.2021.1874854.

Bai, Y., Muralidharan, N., Sun, Y.-K., Passerini, S., Whittingham, M.S., and Belharouak, I. (2020). Energy and environmental aspects in recycling lithium-ion batteries: concept of battery identity global passport. Mater. Today *41*, 304–315. https://doi.org/10.1016/j.mattod.2020.09.001.

Mossali, E., Picone, N., Gentilini, L., Rodriguez, O., Pérez, J.M., and Colledani, M. (2020). Lithium-ion batteries towards circular economy: a literature review of opportunities and issues of recycling treatments. J. Environ. Manage. *264*, 110500. https://doi.org/10.1016/j.jenvman.2020.110500.

Chen, M., Ma, X., Chen, B., Arsenault, R., Karlson, P., Simon, N., and Wang, Y. (2019). Recycling end-of-life electric vehicle lithium-ion batteries. Joule *3*, 2622–2646. https://doi.org/10.1016/j.joule.2019.09.014.

Du, K.D., Ang, E.H., Wu, X.L., and Liu, Y. (2021). Progresses in sustainable recycling technology of spent lithium-ion batteries. Energy Environ. Mater. https://doi.org/10.1002/eem2.12271.

Ciez, R.E., and Whitacre, J.F. (2019). Examining different recycling processes for lithium-ion batteries. Nat. Sustain. *2*, 148–156. https://doi.org/10.1038/s41893-019-0222-5.

Mansur, M.B., Guimarães, A.S., and Petraniková, M. (2021). An overview on the recovery of cobalt from end-of-life lithium ion batteries. Miner. Process. Extr. Metall. Rev. 1–21. https://doi.org/10.1080/08827508.2021.1883014.

Atia, T.A., Elia, G., Hahn, R., Altimari, P., and Pagnanelli, F. (2019). Closed-loop hydrometallurgical treatment of end-of-life lithium ion batteries: towards zero-waste process and metal recycling in advanced batteries. J. Energy Chem. *35*, 220–227. https://doi.org/10.1016/j.jechem.2019.03.022.

Velázquez-Martínez, O., Valio, J., Santasalo-Aarnio, A., Reuter, M., and Serna-Guerrero, R. (2019). A critical review of lithium-ion battery recycling processes from a circular economy perspective. Batteries *5*. https://doi.org/10.3390/batteries5040068.

Zhang, X., Li, L., Fan, E., Xue, Q., Bian, Y., Wu, F., and Chen, R. (2018a). Toward sustainable and systematic recycling of spent rechargeable batteries. Chem. Soc. Rev. *47*, 7239–7302. https://doi.org/10.1039/C8CS00297E.

Li, L., Zhang, X., Li, M., Chen, R., Wu, F., Amine, K., and Lu, J. (2018a). The recycling of spent lithium-ion batteries: a review of current processes and technologies. Electrochem. Energy Rev. *1*, 461–482. https://doi.org/10.1007/s41918-018-0012-1.

Gao, W., Zhang, X., Zheng, X., Lin, X., Cao, H., Zhang, Y., and Sun, Z.H.I. (2017). Lithium carbonate recovery from cathode scrap of spent lithium-ion battery: a closed-loop process. Environ. Sci. Technol. *51*, 1662–1669. https://doi.org/10.1021/acs.est.6b03320.

Yang, T., Lu, Y., Li, L., Ge, D., Yang, H., Leng, W., Zhou, H., Han, X., Schmidt, N., Ellis, M., and Li, Z. (2020). An effective relithiation process for recycling lithium-ion battery cathode materials. Adv. Sustain. Syst. *4*, 1900088. https://doi.org/10.1002/adsu.201900088.

Xu, P., Dai, Q., Gao, H., Liu, H., Zhang, M., Li, M., Chen, Y., An, K., Meng, Y.S., Liu, P., et al. (2020). Efficient direct recycling of lithium-ion battery cathodes by targeted healing. Joule *4*, 2609–2626. https://doi.org/10.1016/j.joule.2020.10.008.

Li, J., Lu, Y., Yang, T., Ge, D., Wood, D.L., III, and Li, Z. (2020). Water-based electrode manufacturing and direct recycling of lithium-ion battery electrodes—a green and sustainable manufacturing system. iScience *23*, 101081. https://doi.org/10.1016/j.isci.2020.101081.

Larouche, F., Tedjar, F., Amouzegar, K., Houlachi, G., Bouchard, P., Demopoulos, G.P., and Zaghib, K. (2020). Progress and status of hydrometallurgical and direct recycling of Li-ion batteries and beyond. Materials *13*, 801. https://doi.org/10.3390/ma13030801.

Sloop, S.E., Trevey, J.E., Gaines, L., Lerner, M.M., and Xu, W. (2018). Advances in direct recycling of lithium-ion electrode materials. ECS Trans. *85*, 397. https://doi.org/10.1149/08513.0397ecst.

Fan, M., Chang, X., Guo, Y.-J., Chen, W.-P., Yin, Y.-X., Yang, X., Meng, Q., Wan, L.-J., and Guo, Y.-G. (2021). Increased residual lithium compounds guided design for green recycling of spent lithium-ion cathodes. Energy Environ. Sci. *14*, 1461–1468. https://doi.org/10.1039/D0EE03914D.

Liang, H.-J., Hou, B.-H., Li, W.-H., Ning, Q.-L., Yang, X., Gu, Z.-Y., Nie, X.-J., Wang, G., and Wu, X.-L. (2019). Staging Na/K-ion de-/intercalation of graphite retrieved from spent Li-ion batteries: in operando X-ray diffraction studies and an advanced anode material for Na/K-ion batteries. Energy Environ. Sci. *12*, 3575–3584. https://doi.org/10.1039/C9EE02759A.

Divya, M.L., Natarajan, S., Lee, Y.S., and Aravindan, V. (2020). Highly reversible Na-intercalation into graphite recovered from spent Li–ion batteries for high-energy Na-ion capacitor. ChemSusChem *13*, 5654–5663. https://doi.org/10.1002/cssc.202001355.

Meng, Y.-F., Liang, H.-J., Zhao, C.-D., Li, W.-H., Gu, Z.-Y., Yu, M.-X., Zhao, B., Hou, X.-K., and Wu, X.-L. (2022). Concurrent recycling chemistry for cathode/anode in spent graphite/LiFePO4 batteries: designing a unique cation/anion-co-workable dual-ion battery. J. Energy Chem. *64*, 166–171. https://doi.org/10.1016/j.jechem.2021.04.047.

Li, M., Lu, J., Chen, Z., and Amine, K. (2018b). 30 Years of lithium-ion batteries. Adv. Mater. *30*, 1800561. https://doi.org/10.1002/adma.201800561.

Mizushima, K., Jones, P.C., Wiseman, P.J., and Goodenough, J.B. (1980). A new cathode material for batteries of high energy density. Mater. Res. Bull *15*, 783–789. https://doi.org/10.1016/0025-5408(80)90012-4.

Lyu, Y., Wu, X., Wang, K., Feng, Z., Cheng, T., Liu, Y., Wang, M., Chen, R., Xu, L., Zhou, J., et al. (2021). An overview on the advances of LiCoO2 cathodes for lithium-ion batteries. Adv. Energy Mater. *11*, 2000982. https://doi.org/10.1002/aenm.202000982.

Ding, Y., Cano, Z.P., Yu, A., Lu, J., and Chen, Z. (2019). Automotive Li-ion batteries: current status and future perspectives. Electrochem. Energy Rev. *2*, 1–28. https://doi.org/10.1007/s41918-018-0022-z.

Noh, H.-J., Youn, S., Yoon, C.S., and Sun, Y.-K. (2013). Comparison of the structural and electrochemical properties of layered Li [NixCoyMnz] O2 (x= 1/3, 0.5, 0.6, 0.7, 0.8 and 0.85) cathode material for lithium-ion batteries. J. Power Sourc. *233*, 121–130. https://doi.org/10.1016/j.jpowsour.2013.01.063.

Yoon, C.S., Choi, M.H., Lim, B.-B., Lee, E.-J., and Sun, Y.-K. (2015). Review—high-capacity Li[Ni1-xCox/2Mnx/2]O2(x= 0.1, 0.05, 0) cathodes for next-generation Li-ion battery. J. Electrochem. Soc. *162*, A2483–A2489. https://doi.org/10.1149/2.0101514jes.

Kim, U.-H., Park, N.-Y., Park, G.-T., Kim, H., Yoon, C.S., and Sun, Y.-K. (2020). High-energy W-doped Li [Ni0. 95Co0. 04Al0. 01] O2 cathodes for next-generation electric vehicles. Energy Storage Mater *33*, 399–407. https://doi.org/10.1016/j.ensm.2020.08.013.

Beaudet, A., Larouche, F., Amouzegar, K., Bouchard, P., and Zaghib, K. (2020). Key challenges and opportunities for recycling electric vehicle battery materials. Sustainability *12*, 5837. https://doi.org/10.3390/su12145837.

Zhang, L., Mu, Z., and Sun, C. (2018b). Remaining useful life prediction for lithium-ion batteries based on exponential model and particle filter. IEEE Access *6*, 17729–17740. https://doi.org/10.1109/ACCESS.2018.2816684.

Shi, Y., Zhang, M., Meng, Y.S., and Chen, Z. (2019). Ambient-pressure relithiation of degraded LixNi0.5Co0.2Mn0.3O2 (0 < x < 1) via eutectic solutions for direct regeneration of lithium-ion battery cathodes. Adv. Energy Mater. *9*, 1900454. https://doi.org/10.1002/aenm.201900454.

Li, L., Deng, J., Chen, J., and Xing, X. (2016). Topochemical molten salt synthesis for functional perovskite compounds. Chem. Sci. *7*, 855–865. https://doi.org/10.1039/C5SC03521J.

Yuan, Y., Xiao, W., Wang, Z., Fray, D.J., and Jin, X. (2018). Efficient nanostructuring of silicon by electrochemical alloying/dealloying in molten salts for improved lithium storage. Angew. Chem. Int. Ed. *57*, 15743–15748. https://doi.org/10.1002/anie.201809646.

Parnham, E.R., and Morris, R.E. (2007). Ionothermal synthesis of zeolites, metal–organic frameworks, and inorganic–organic hybrids. Acc. Chem. Res. *40*, 1005–1013. https://doi.org/10.1021/ar700025k.

Mesnier, A., and Manthiram, A. (2020). Synthesis of LiNiO2 at moderate oxygen pressure and long-term cyclability in lithium-ion full cells. ACS Appl. Mater. Inter. *12*, 52826–52835. https://doi.org/10.1021/acsami.0c16648.

Ganter, M.J., Landi, B.J., Babbitt, C.W., Anctil, A., and Gaustad, G. (2014). Cathode refunctionalization as a lithium ion battery recycling alternative. J. Power Sourc. *256*, 274–280. https://doi.org/10.1016/j.jpowsour.2014.01.078.

Onofre, P.N.R. (2019). Evaluation of Pyrochemistry in Molten Salts for Recycling Li-Ion Batteries (Sorbonne Université).

STAR★METHODS

KEY RESOURCES TABLE

REAGENT or RESOURCE	SOURCE	IDENTIFIER
Chemicals, peptides, and recombinant proteins		
Sodium Hydroxide	Thermo Scientific	CAS 1310-73-2
Lithium Hydroxide	Fisher Chemical	CAS 1310-65-2
Nickel(II) nitrate hexahydrate	Thermo Scientific	CAS 13478-00-7
Lithium choloride	Fisher Chemical	CAS 7447-41-8
Sodium nitrate	Sigma-Aldrich	CAS 7631-99-4
Lithium nitrate	Sigma-Aldrich	CAS 7790-69-4
Nickel(II) choloride hexahydrate	Thermo Scientific	CAS 13478-00-7
NMC 111	BASF TODA Battery Materials LLC	provided by CAMP at Argonne National Laboratory
NMC 622	BASF TODA Battery Materials LLC	provided by CAMP at Argonne National Laboratory
NMC 811	BASF TODA Battery Materials LLC	provided by CAMP at Argonne National Laboratory
Delithiated NMC 111 (D-NMC 111)	supplied by Dr. Pupek,Dr. Dahl Dr. Polzin at the MERF facility	
N-methylpyrrolidone (NMP)	Sigma-Aldrich	CAS 872-50-4
Graphite	Superior Graphite	Superior SLC1520T
Poly(vinylidene fluoride) (PVDF)	MSE Supplies	CAS 24937-79-9
1.2 M $LiPF_6$ in 3:7 wt% ethylene carbonate/ ethyl methylcarbonate	Soulbrain MI	
Lithium ribbon	Sigma-Aldrich	CAS 7439-93-2
Software and algorithms		
Neware BTS Data Analysis	Neware Technology Limited	7.6.0.255
Origin 2018 64bit SR1	OriginLab Corporation	b9.5.1.195

RESOURCE AVAILABILITY

Lead contact

Further information and requests for resources should be directed to and will be fulfilled by the Lead Contact, Sheng Dai (dais@ornl.gov).

Materials availability

This study did not generate new unique reagents.

Data and code availability

- All data reported in this paper will be shared by the lead contact upon request.
- This paper does not report original code.
- Any additional information required to reanalyze the data reported in this paper is available from the lead contact upon request.

METHOD DETAILS

Upcycling procedures

The delithiated NMC 111 (D-NMC 111) was provided by Argonne National Lab, which is obtained by a chemical delithiation using the NO2BF4 oxidizer.[7] For the upcycling of D-NMC 111 to NMC 622 in

RTMS system, 1.0 g of D-NMC 111 was mixed with 2.4 g of $Ni(NO_3)_2 \cdot 6H_2O$ and 0.86 g of LiCl by hand grinding in an agate mortar. After grinding, the mixture became a slurry, to which 1.2 g of NaOH was added and then grided until a uniform soil formed. Then the upcycling mixture was dried at 110 °C overnight in a vacuum oven, grided into fine powder before heating in a muffle furnace. The mixture was heated to 300 °C for 5 h and to 800 °C for 5 h with a heating rate of 5 °C/min in air. After cooling down to ambient temperature, the mixture was washed with water by vacuum filtration to remove salts, dried at 110 °C overnight in a vacuum oven, and heated to 600 °C for 2 h with a heating rate of 5 °C/min in air to obtain the final product Up-NMC 622.

For control experiments using $NaNO_3/LiNO_3$ binary molten salts, LiCl in upcycling mixture was replaced by equimolar $LiNO_3$. For NaCl/LiCl binary molten salts, $Ni(NO_3)_2 \cdot 6H_2O$ was replaced by equimolar $NiCl_2 \cdot 6H_2O$. For $LiCl/LiNO_3$ binary molten salts, NaOH was replaced by equimolar LiOH. The dry and heating processes in control experiments were same to RTMS upcycling processes.

Electrochemical measurements

The NMC cathode slurry contains NMC, carbon black, and 5 wt% binder polyvinylidene difluoride (PVDF) with a mass ratio of 90:5:5, and appropriate amount of N-methylpyrrolidone (NMP). Cathodes were casted on Al foil at a total loading of around 8.6 mg/cm^2. For full cell tests, the anode slurry containing graphite, and carbon black with a mass ratio of 92:6:2, and NMP was coated on Cu foil. All electrodes were dried at 110 °C overnight in a vacuum oven prior to cell assembly. For half-cell tests, Li foil disks were used as anodes. All the coin cells were assembled in an argon-filled glove box using one layer of Celgard 2325 membrane as the separator and 120 μL of 1.2 M $LiPF_6$ in 3:7 wt% ethylene carbonate/ethyl methylcarbonate as the electrolyte. 10 h of rest was performed for all coin cells before cycling. All cells were tested under ambient temperature. The voltage windows were 3.0 ~ 4.3 V and 3.0 ~ 4.2 V vs. Li/Li^+ for half-cell and full cell tests, respectively. Four formation cycles were performed at a specific current of 20 mA/g charge/discharge before cycling at 200 mA/g for 100 cycles. Full cells were charged using a CCCV protocol (charged to 4.2 V using a constant specific current of 200 mA/g, then held at 4.2 V until the current dropped to 66 mA/g before discharging).

Characterizations

Thermogravimetric analysis (TGA) for NMCs was performed on a TGA 2950, TA Instruments by heating from room temperature to 800 °C at a rate of 10 °C/min in air. TGA/DTA data of the upcycling mixture was collected by STA300, HITACHI, using a heating rate of 5 °C/min from room temperature to 800 °C in air. Scanning electron microscope (SEM) images were captured on a ZEISS AURIGA CROSSBEAM FIB. X-ray diffraction (XRD) patterns were collected by a PANalytical Empyrean diffractometer, operated at 45 kV and 40 mA using Cu Kα (λ = 0.1542 nm). Inductively coupled-plasma optical emission spectroscopy (ICP-OES) for the elemental analysis was performed on an Agilent 5110 ICP-OES spectrometer. X-ray photoelectron spectroscopy (XPS) experiments were performed with a PHI 3056 spectrometer equipped with an Al anode source operated at 15 KV with an applied power of 350 W and a pass energy of 93.5 eV.

QUANTIFICATION AND STATISTICAL ANALYSIS

Figures represent averaged or representative results of multiple independent experiments. Analyses and plots were performed with Origin.